Fine-Scale Zonal Flow Suppression of Electron Temperature Gradient Turbulence

S.E. Parker*, J.J. Kohut*, Y. Chen*, Z. Lin†, F.L. Hinton** and W.W. Lee‡

*Center for Integrated Plasma Studies, University of Colorado, Boulder,C0
†University of Californian, Irvine, CA
**Hinton Associates, Escondido, CA
‡Princeton Plasma Physics Laboratory, Princeton, NJ

Abstract. It is found in collisionless Electron Temperature Gradient (ETG) turbulence simulations that, while zonal flows are weak at early times, the zonal flows continue to grow algebraically (proportional to time). These fine-scale zonal flows have a radial wave number such that $k_r\rho_i > 1$ and $k_r\rho_e < 1$. Eventually, the zonal flows grow to a level that suppresses the turbulence due to ExB shearing. The final electron energy flux is found to be relatively low. These conclusions are based on particle convergence studies with adiabatic ion electrostatic flux-tube gyrokinetic δf particle simulations run for long times. The Rosenbluth-Hinton random walk mechanism is given as an explanation for the long time build up of the zonal flow in ETG turbulence and it is shown that the generation is $(k_\perp\rho_e)^2$ smaller than for isomorphic Ion Temperature Gradient (ITG) problem. This mechanism for zonal flow generation here is different than the modulational instability mechanism for ITG turbulence. These results are important because previous results indicated zonal flows were unimportant for ETG turbulence. Weak collisional damping of the zonal flow is also shown to be a n important effect.

Keywords: plasma, transport, gyrokinetic, turbulence
PACS: 52.35.Ra, 52.35.Kt, 52.65.-y

INTRODUCTION

Gyrokinetic continuum simulation studies of electron temperature gradient (ETG) turbulence have seen significant electron heat transport levels, $\chi_e > 10\rho_e^2 v_{te}/L_T$[1, 2, 3]. Though the wavelength of ETG turbulence in the θ direction is on the ρ_e scale, $k_\theta\rho_e \sim 0.2$, radially elongated eddies are observed that can cause quite large transport. Unlike ion-temperature-gradient (ITG) turbulence, zonal flows have been so far shown to be weak[1] so the radially elongated eddies persist. More recent studies of ETG turbulence using a global gyrokinetic particle simulation show heat transport levels that are much lower[4, 5]. These results have come under scrutiny because similar flux-tube simulations appear to be noise dominated[6]. Additionally, continuum simulation results using differernt pararmeters have observed lower electron heat flux levels as well[7].

Presented here, are findings after performing particle convergence studies using an electrostatic three-dimensional toroidal flux-tube simulation with adiabatic ions (the typical limit for ETG turbulence studies). It is found that even though zonal flows are relatively weak for early times after initial nonlinear saturation, the zonal flows grow algebraically in time via the Rosenbluth-Hinton random walk mechanism[8, 9]. The zonal flows eventually grow to a level where ExB shear flow suppression[10, 11] becomes important. ETG turbulence is susceptible to shear suppression because of the

CP871, *Theory of Fusion Plasmas: Joint Varenna-Lausanne International Workshop,*
edited by J. W. Connor, O. Sauter, and E. Sindoni

large radial extent of the eddies[4]. The diffusive growth of the zonal flows is due to chaotic turbulent fluctuations in the ExB source term[8, 9]. Without collisional damping, the zonal flows grow to high levels.

THE GEM GYROKINETIC TURBULENCE SIMULATION CODE

GEM is a global gyrokinetic turbulence simulation using the δf particle-in-cell method[12, 13]. GEM uses realistic equilibrium profiles and arbitrary axisymetric magnetic equilibria[12]. Electrons can be either drift-kinetic, gyrokinetic or adiabatic and ions are either gyrokinetic or adiabatic. GEM includes perpendicular magnetic perturbations (electromagnetic), electron-ion collisions, equilibrium shear flow, and minority species ions. For the electrostatic ETG simulations presented here, the electrons are gyrokinetic and the ions are assumed to be adiabatic.

PARTICLE CONVERGENCE STUDIES OF ETG SIMULATION

Fig. 1 shows the electron heat diffusivity for seven simulations, varying the number of particles per cell from 8 to 512. The physical parameters are the the so-called “Cyclone base-case"[14, 15] except with the temperature gradient reduced 30% to $R/L_T = 5.3$. Specifically, the parameters are: $R/L_T = 5.3$, $q = 1.4$, $\hat{s} = 0.8$, $R/L_n = 2.2$, $T_i = T_e$, $r/R = 0.18$, $\Delta t = 0.1 v_{te}/L_T$, $\Delta x = \Delta y = 2\rho_e$, $L_x = 256\rho_e$, $L_y = 128\rho_e$, the grid is $128 \times 64 \times 32$. Simulations with a $256 \times 128 \times 32$ grid and $\Delta x = \Delta y = \rho_e$ show similar behavior. The number of tracer particles was varied from 2,097,152 to 134,217,728. The reason for reducing the temperature gradient by 30% from the Cyclone bas-case value was because of lack of both clear nonlinear saturation and a stationary state. We will present a R/L_T scan and discuss the problems with the $R/L_T = 6.9$ case in the "Summary and Discussion" section. For the $R/L_T = 5.3$ case the flux eventually drops to much lower levels, qualitatively similar to Lin, et al.[4, 5]. Fig. 1 shows that the flux drop does not occur later for increased particle number, which would otherwise be a signature of the noise effect of Nevins, et al.[6]. In fact, the drop occurs earlier for larger particle number and we conclude the low flux result is physical.

ELECTRON-SCALE ZONAL FLOWS

Fig. 2 shows contours of the electrostatic potential in the perpendicular plane. The x-coordinate is the radial coordinate $r - r_0$ and the y-coordinate is the toroidal coordinate, see Ref. [12] for simulation model details. Fig. 2 shows snapshots of the $\phi(x,y,z=0)$ at $tv_{te}/L_T = 647$ and $tv_{te}/L_T = 2835$ for the $R/L_T = 5.3$, 128 particles per cell case. It is observed that the purely radial modes (or zonal flows) are dominant. The individual Fourier modes of the flux-surface-averaged electrostatic potential $| < \phi > |_k$ for the same case are shown in the lower figure of Fig. 3, where $k = 2n\pi/L_x$ and the mode numbers n are labeled. The electron heat diffusivity versus time is shown in the upper figure of Fig. 3 for time reference. We can make an estimate of when the zonal flow ExB shear

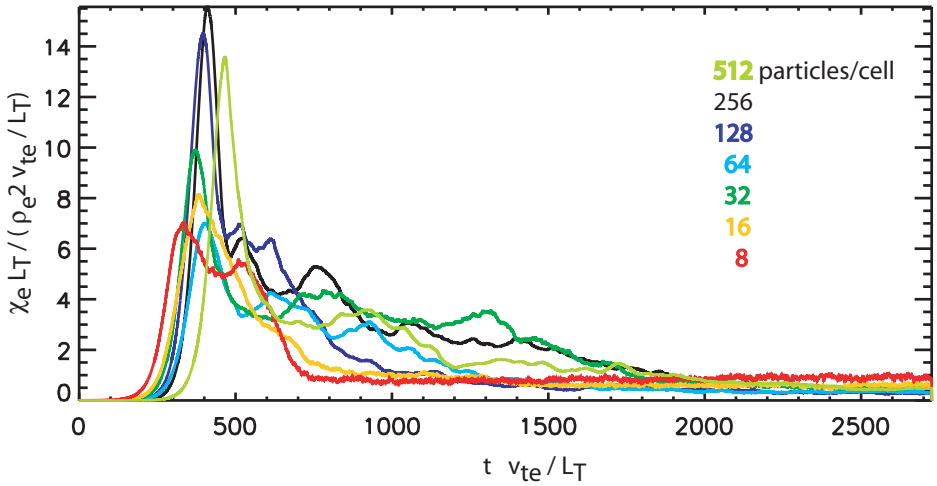

FIGURE 1. Electron thermal diffusivity for $R/L_T = 5.3$ case with 16, 32, 64, 128, 256 and 512 particles per cell. Qualitative behavior similar to Lin, et al.[4, 5].

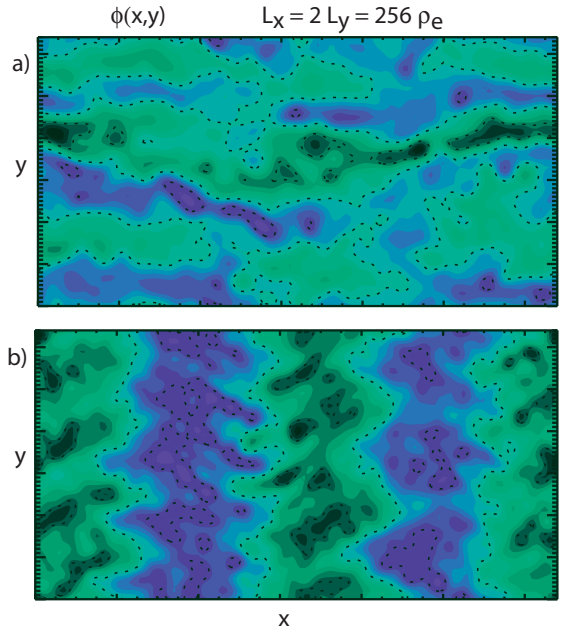

FIGURE 2. $R/L_T = 5.3$, 128 particles per cell case showing snapshots of the $\phi(x,y,z=0)$ at a) $tv_{te}/L_T = 647$ and b) $tv_{te}/L_T = 2385$. Purely radial electric fields are evident at late times.

suppression becomes significant using the ExB shearing rate criterion[11], $\omega_{sh} > \Delta\omega_T$, where $\omega_{sh} = (\Delta r/\Delta\theta)\, k_r^2 | < \phi > |_k / B$, ω_{sh} is the shearing rate, $\Delta\omega_T$ is the scattering rate of the background turbulence [11] ($\Delta\omega$ of the turbulence), $\Delta\theta$ is the poloidal correlation length and Δr is the radial correlation length of the ambient turbulence (subtracting out the purely radial modes). k_r is the wavenumber of the zonal flow and $| < \phi > |_k$ is the amplitude of the zonal flow mode under consideration. To estimate the shearing rate we assume $\Delta\omega_T \approx \gamma$ where $\gamma L_T / v_{te} = 0.018$ is the measured linear growth rate. We also

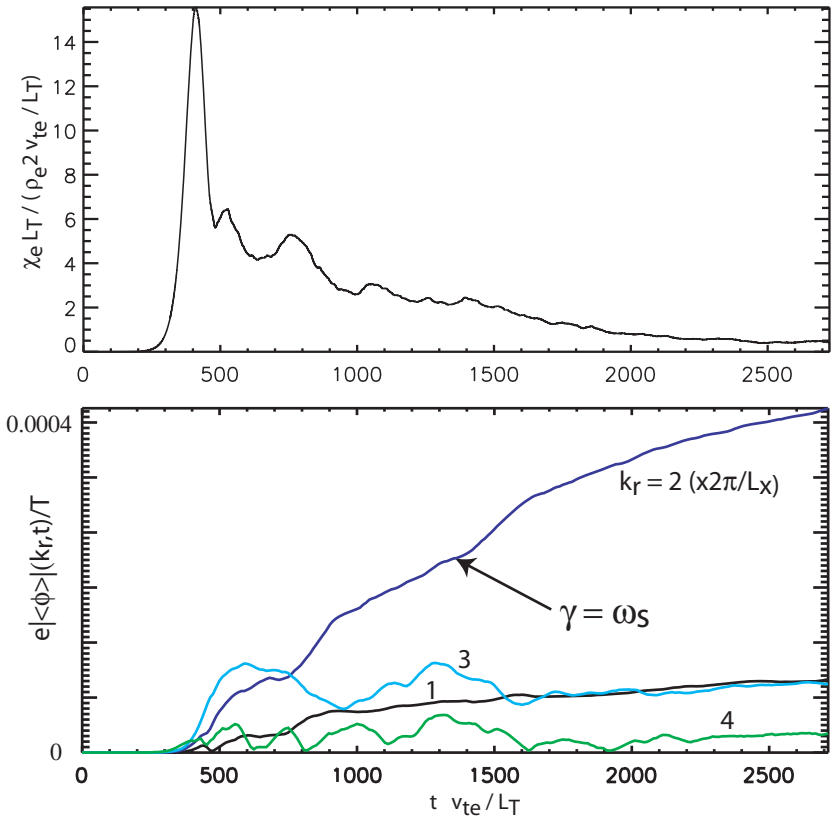

FIGURE 3. $R/L_T = 5.3$, 128 particles per cell case showing the time history of the electron thermal diffusivity and the time history of the purely radial electrostatic potential modes. The location where the amplitude of ϕ for the dominant purely radial mode is such that $\gamma = \omega_s$ is shown as well.

take $\Delta r/\Delta\theta = 4$, and $k_r\rho_e = 4\pi\rho_e/L_x = 0.05$ for the the second zonal flow harmonic that dominates. Shown in Fig. 3 is labeled where $\gamma = \omega_{sh}$. Though, this estimate of the shearing rate criterion is approximate, the flux does begin to drop in time when zonal flow gets in a level such that ExB shearing becomes significant.

Also carried out were simulations where the zonal flows were set to zero. In simulations where we zero out the purely radial electrostatic potential, the electron heat flux stays 5-40 times higher as shown in Fig. 4. We conclude that the flux drops to very low levels due to the background turbulence providing a random source that drives algebraic growth of the zonal flows that eventually shear suppress the underlying turbulence.

Next, a R/L_T scan is presented in Fig. 5. One observes a supercritical gradient region, analogous to the "Dimits Shift"[15, 14] that is found for ITG turbulence. In the range of $R/L_T = 4.5 - 5.3$ the heat flux is quite small, even though the plasma is well above the linear threshold. Larger values of R/L_T that are not shown in Fig. 5 exhibit difficulties achieving a clean nonlinear saturation at higher grid resolution. These stronger gradient cases will be addressed in the "Summary and Discussion" section. χ_e is measured by averaging the electron heat flux from 2000 to 2300 L_T/v_{te}. An important observation is that in the higher flux cases i.e. $R/L_T > 5.3$, the flux continues to drop and the zonal flow continues to build. The results of Fig. 5 are sensitive to the time where χ_e time averaged.

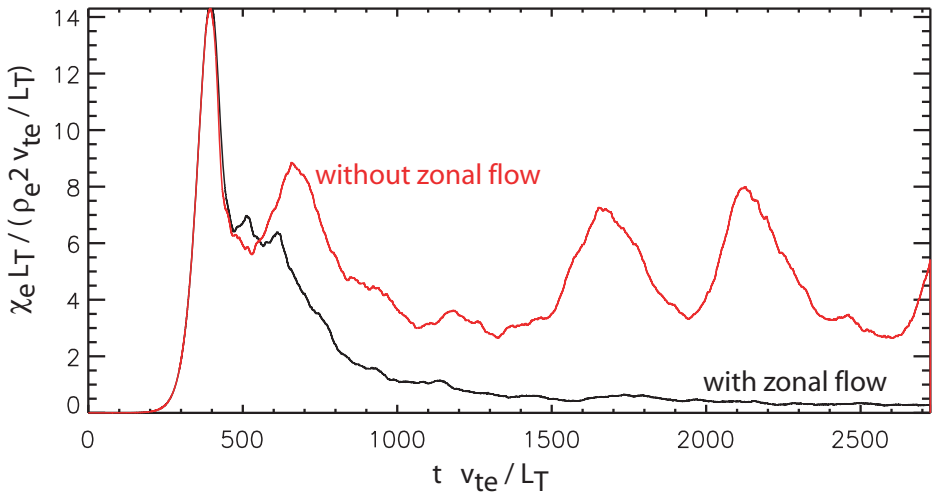

FIGURE 4. $R/L_T = 5.3$, 128 particles per cell case with and without the zonal flows. The lower line is the electron heat diffusivity for the original case. The upper line shows the same simulation with $< \phi >$ zeroed out.

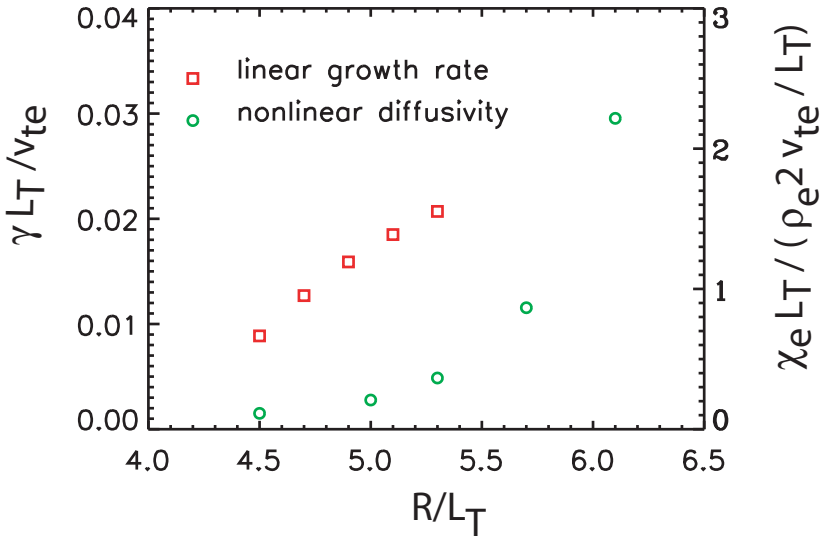

FIGURE 5. R/L_T scan showing χ_e drops to very low values at linearly unstable values. Qualitatively similar to the super-critical gradient region in ITG.

Fig. 6 shows the time history of χ_e for the $R/L_T = 5.3$ (black), 5.7 (orange) and 6.1 (blue) case. As an example of the continued zonal flow build up, the time histories of the zonal flow modes for the $R/L_T = 6.1$ case are shown in Fig. 7.

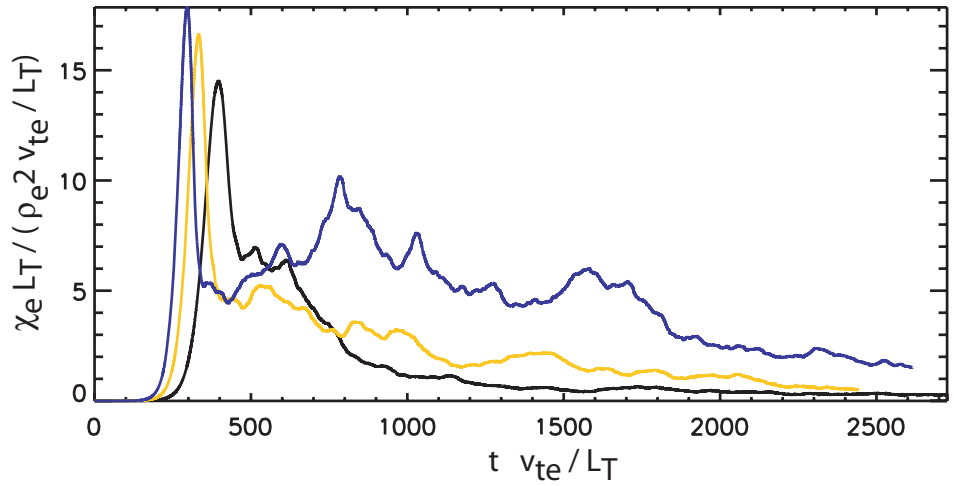

FIGURE 6. χ_e time histories of the $R/L_T = 5.3$ (lowest line), 5.7 (middle line) and 6.1 (highest line) simulations. The χ_e versus R/L_T is obtained in Fig. 5 by time averaging towards the end of the run. However, χ_e continues to drop at later times and zonal flows continue to grow (for the 5.7 and 6.1 case).

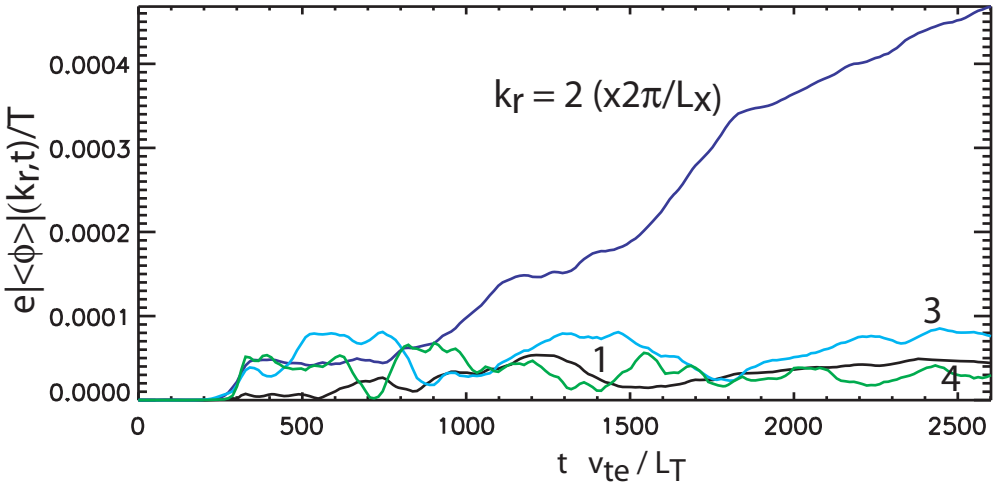

FIGURE 7. Zonal flow mode time histories for the $R/L_T = 6.1$ case, showing continued zonal flow build up at late times.

COLLISIONAL DAMPING OF ELECTRON SCALE ZONAL FLOWS

Like in ITG turbulence, collisions and/or anomalous viscosity could set the final level of the zonal flow[8, 9, 16]. An immediate question is: could anomalous viscosity or collisional damping may become important before shear suppression becomes significant? Anomalous viscous damping of the zonal flow did not appear to be significant in the collisionless $R/L_T = 5.3$ case, in that the zonal flow continued to grow until shear suppression took place. Following from Rosenbluth and Hinton's work on ITG zonal flow

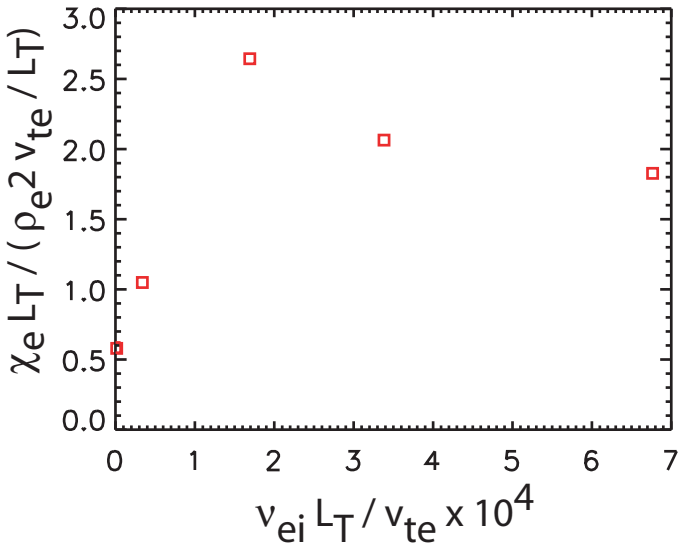

FIGURE 8. χ_e versus collisionality showing weak collisionality changes the level of electron heat flux.

dynamics[8, 9], the corresponding ETG model equation is

$$\frac{\partial}{\partial t}|\phi_k|^2 = A_k|S|^2 - C_k|\phi_k|^2|S|^2 - D_k\nu_{ei}|\phi_k|^2, \tag{1}$$

(see Eq. (19) in Ref. [8]) where the first term is the ExB source term (we will discuss this term further below), the second term is turbulent viscosity, and the third term is the electron-ion collisional damping. Hence, one might expect collisional damping to be important in setting the zonal flow level, thereby, influencing the electron heat flux. This indeed appears to be the case.

Fig. 8 shows χ_e versus ν_{ei}, where χ_e is measured by averaging from from 1300 to 1500 L_T/v_{te}. $R/L_T = 5.3$ and 128 particles per cell are used. For this range of collisionality, there is little affect on the linear growth rate since $\gamma \gg \nu_{ei}$. The initial nonlinear saturation is affected by these weak levels of collisionality, and this may play a roll in the non-monotonic behavior of χ_e versus ν_{ei}. Fig. 9 shows the corresponding χ_e time histories for the four collisional cases shown in Fig. 8. Finally, Fig. 10 shows the zonal flow mode histories for $\nu_{ei}L_T/v_{te} = 0.34 \times 10^{-4}$ (top) and $\nu_{ei}L_T/v_{te} = 3.4 \times 10^{-4}$ (bottom). Though, the actual level is only 10% lower for second harmonic at the termination of the run for the more collisional case, the initial growth is significantly lower. The other cases also showed slower growth and a lower overall level at the termination of the run. $\nu_{ei}L_T/v_{te} = 1.7 \times 10^{-4}$ showed a 55% drop and $\nu_{ei}L_T/v_{te} = 6.8 \times 10^{-4}$ showed a 28% drop.

ELECTRON-SCALE ZONAL FLOW DYNAMICS

One observation, is that while all the zonal flow modes typically grow slowly in time, the second harmonic dominates. This may be explained by the fact that the dominant radial

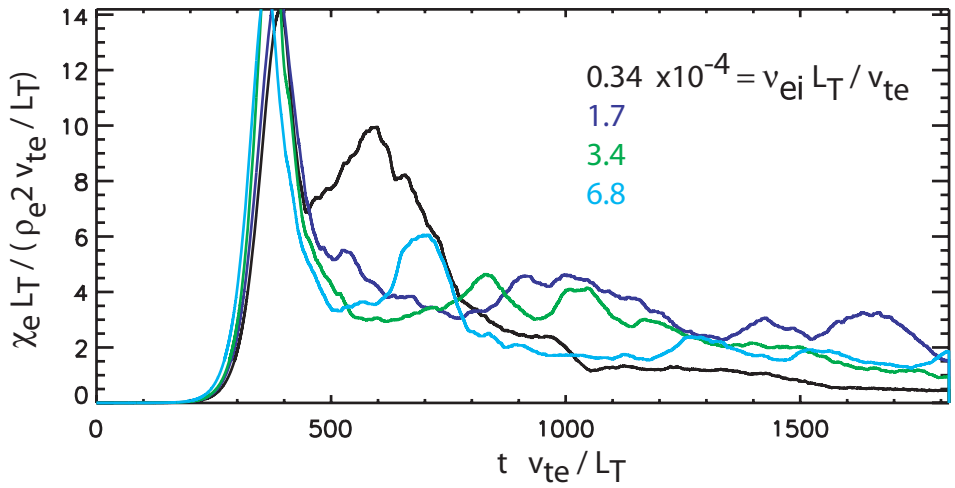

FIGURE 9. χ_e versus time for the four collisoinal runs.

mode of the background turbulence is $k_r = 0$ and the fundamental radial mode. The $k_r = 0$ does not contribute to the purely radial modes through mode coupling via the ExB nonlinearity. So, then a significant coupling would be $(1, \pm m, \pm n) + (1, \mp m, \mp, n) \rightarrow (2, 0, 0)$.

To examine the behavior of the zonal flows, we take the slab gyrofluid equations assuming $(k_\perp \rho)^2 \ll 1$, $T_i = T_e$, using units $x \rightarrow x/\rho$, $t \rightarrow t\omega_c$, and $v \rightarrow v/v_t$. The electron quasi-neutrality condition, the guiding center continuity equation, and the simplest guiding center perpendicular temperature equation are[17, 14, 1]

$$\left(1 - \nabla_\perp^2\right)\phi = \left(1 + \nabla_\perp^2\right) n + \frac{1}{2}\nabla_\perp^2 T_\perp, \tag{2}$$

$$\frac{\partial}{\partial t} n + \mathbf{v_E} \cdot \nabla n + \frac{1}{2}\nabla_\perp^2 \mathbf{v_E} \cdot \nabla T_\perp = 0, \tag{3}$$

$$\frac{\partial}{\partial t} T_\perp + \mathbf{v_E} \cdot \nabla T_\perp = 0. \tag{4}$$

For ITG, the ion gyrofluid equations are a very similar form except for the zero electron response for the purely radial electrostatic potential. Tildes are used to signify the ion equations.

$$(\tilde{\phi} - < \tilde{\phi} >) - \nabla_\perp^2 \tilde{\phi} = \left(1 + \nabla_\perp^2\right) \tilde{n} + \frac{1}{2}\nabla_\perp^2 \tilde{T}_\perp, \tag{5}$$

$$\frac{\partial}{\partial t} \tilde{n} + \mathbf{v_E} \cdot \nabla \tilde{n} + \frac{1}{2}\nabla_\perp^2 \mathbf{v_E} \cdot \nabla \tilde{T}_\perp = 0, \tag{6}$$

$$\frac{\partial}{\partial t} \tilde{T}_\perp + \mathbf{v_E} \cdot \nabla \tilde{T}_\perp = 0. \tag{7}$$

Combining Eqs.(2)-(4), we obtain an evolution equation for the zonal flows, for ETG

$$\frac{\partial}{\partial t} < \phi >_k = -k_r^2 \frac{\partial}{\partial t} < T_\perp >_k + \left\langle \mathbf{v_E} \cdot \nabla \nabla_\perp^2 \left(2\phi + \frac{1}{2} T_\perp\right) \right\rangle_k. \tag{8}$$

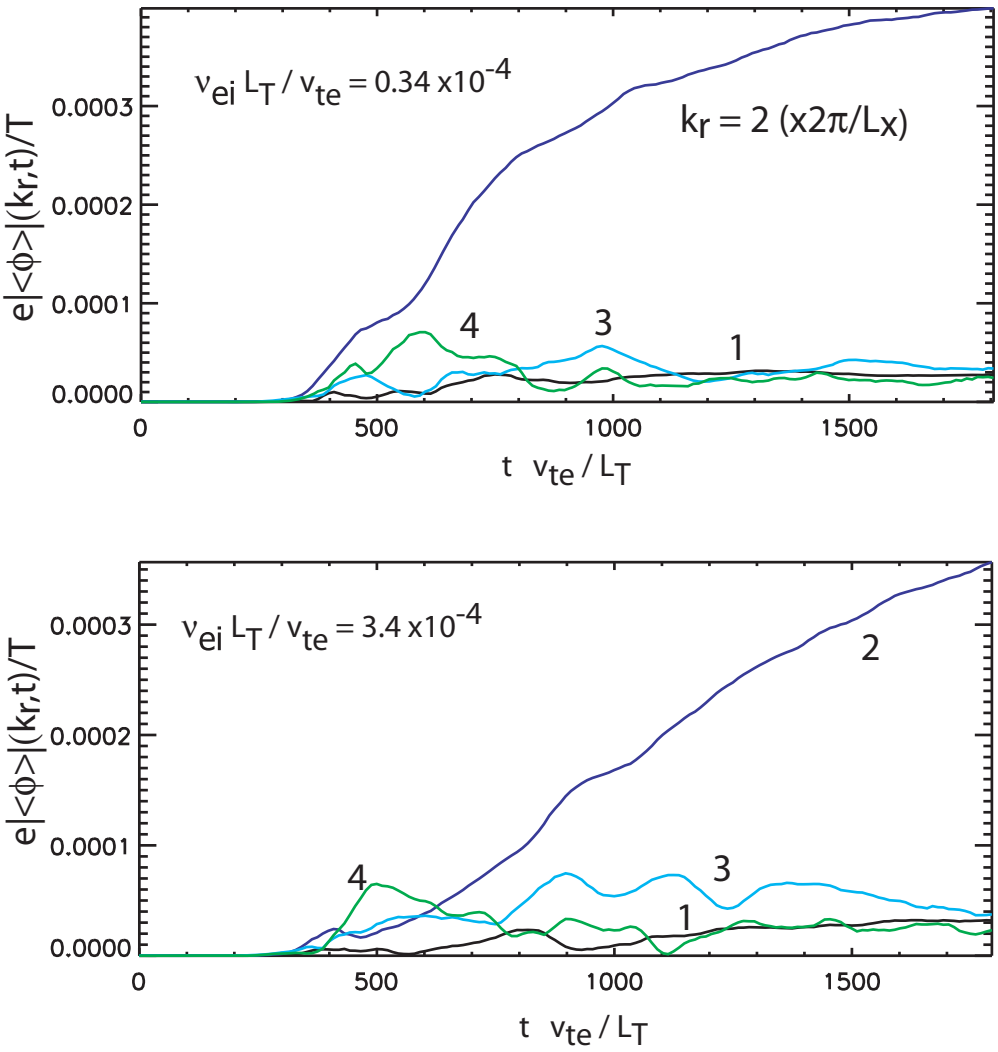

FIGURE 10. Zonal flow mode histories for the collisional cases $\nu_{ei}L_T/v_{te} = 0.34 \times 10^{-4}$ (top) and $\nu_{ei}L_T/v_{te} = 3.4 \times 10^{-4}$ (bottom).

For ITG, combining Eqs. (5)-(7) the analogous equation governing the zonal flows is

$$\frac{\partial}{\partial t} < \tilde{\phi} >_k = -\frac{\partial}{\partial t} < \tilde{T}_\perp >_k - \frac{1}{2k_r^2} \left\langle \mathbf{v_E} \cdot \nabla \nabla_\perp^2 \left(\tilde{\phi} + \frac{1}{2} \tilde{T}_\perp \right) \right\rangle_k . \tag{9}$$

From Eq. (8) and (9) it is evident that the ETG zonal flow generation is $(k_r\rho)^2$ weaker than the nearly isomorphic ITG case. This explains why initial generation is more important for ITG turbulence where the modulational instability is important during initial nonlinear saturation[18, 16]. However, for ETG the later-time algebraic growth becomes important due to the fact that the fluctuation level is relatively higher. The first term on the right-hand-side of Eqs. (8) and (9) can be cast as an ExB nonlinearity from Eqs.(4) and (7). Hence, the first and second terms on the right-hand-side of Eqs. (7) and

(8) can be combined to form a nonlinear source term of the form $\frac{\partial}{\partial t} < \tilde{\phi} >_k = S_k$, where $S_k \propto |\phi|^2$ like the ExB source term in Eq. (1) and in Refs. [8, 9, 16].

SUMMARY AND DISCUSSION

In summary, we find that for ETG turbulence, zonal flows grow algebraically in time via the Rosenbluth-Hinton diffusive mechanism and eventually suppress the turbulence via ExB shearing. There are many analogs to the well-known zonal flow effect in ITG turbulence, but there is a key difference. Namely, zonal flows grow via the Rosenbluth-Hinton diffusive mechanism[8, 9] and not the modulational instability[18, 16] which is shown here to be weaker by $(k_\perp \rho_e)^2$. The zonal flow reduces the electron heat flux only at late times. This is a new and important result because previously it was predicted that zonal flows were weak and unimportant[1, 2, 3].

For the $R/L_T = 5.3$ case, the zonal flow shear suppressed the turbulence and the electron heat transport level was quite low, $\chi_e < \rho_e^2 v_{te}/L_T$. Finite collisionality is found to be important for experimental tokamak parameters. However, even with collisionality the electron heat flux was relatively low. $R/L_T = 6.1$ was the largest value we could definitively demonstrate the zonal flow suppression mechanism at late times. For larger values of R/L_T, specifically for the $R/L_T = 6.9$ "Cyclone base case", with trapped electrons, we found that the simulation did not saturate well for the finer grid resolution of $256 \times 128 \times 32$ grid, $\Delta x = \Delta y = \rho_e$ and 134 million particles. The coarser grid case with $\Delta x = \Delta y = 2\rho_e$, $L_x = 256\rho_e$, $L_y = 128\rho_e$, did come to a nearly stationary state and showed zonal flow shear stabilization at late times. Since, the ETG turbulence appears to be dominated by longer wavelength modes $k_\perp \rho_e \sim 0.1$, we expect the coarser grid to be adequate even for the $R/L_T = 6.9$ case. But, we cannot exclude the remote possibility that fine grid scale physics is important (e.g. affecting the turbulent viscous damping). At present, we cannot demonstrate convergence with the finer grid because this requires very large (1-10 billion) particle number runs. We expect to do this in the near future on the Cray XT3 at the National Center for Computational Sciences at Oak Ridge National Laboratory.

The fact that the lower gradient $R/L_T = 5.3$ case has qualitative behavior similar to the global gyrokinetic simulation result is not surprising since global effects tend to be linearly stabilizing. Variation of equilibrium quantities localize the resonance radially and fixed boundary conditions localize the mode as well, all linearly stabilizing effects. On the other hand, one would not expect too strong an effect because $\rho_e/L \ll \rho_i/L \ll 1$ and profile variation effects should be weak at fine scales. Accompanying the purely radial electric field is a purely radial pressure perturbation which we have diagnosed and is predicted theoretically, see Eq. (9). In fact, the case without zonal flow initially saturates at moderate levels without zonal flow. Additionally, the simple test of restarting the simulation in the middle of the run with the zonal flow zeroed out requires a transient of $\sim 1000 L_T/v_{te}$ before the flux rises to high levels, indicating an additional saturation mechanism besides simply ExB shearing. A corresponding purely radial pressure perturbation is stabilizing due to diamagnetic shear flow and variation in the natural mode frequency, or the so-called "variation in ω_*" effect[14]. Source terms in global simulations may have an important effect since these terms are designed to damp

out long wavelength purely radial variation of δf. Here, we presented the important result that that zonal flow is actually important for ETG turbulence problem. But, there are clearly other stabilizing effects reducing the flux at long times that need to be further investigated.

ACKNOWLEDGMENTS

Work supported by Department of Energy SciDAC Center for Gyrokinetic Particle Simulation and Center for Plasma Edge Simulation. Thanks to Greg Hammett and Andris Dimits for useful discussion.

REFERENCES

1. W. Dorland, F. Jenko, M. Kotschenreuther, and B. Rogers, *Phys. Rev. Lett.* **85**, 5579 (2000).
2. F. Jenko, W. Dorland, M. Kotschenreuther, and B. Rogers, *Phys. Plasmas* **7**, 1904 (2000).
3. F. Jenko, and W. Dorland, *Phys. Rev. Lett.* **89**, 225001 (2002).
4. Z. Lin, L. Chen, and F. Zonca, *Phys. Plasmas* **12**, 056125 (2005).
5. Z. Lin, L. Chen, Y. Nishimura, H. Qu, T. Hahm, J. Lewandowski, G. Rewoldt, W. Wang, P. Diamond, C. Holland, F. Zonca, and Y. Li, *Plasma Physics and Controlled Nuclear Fusion Research* **IAEA-CN-69**, TH8/1 (2004).
6. W. Nevins, G. Hammett, A. Dimits, W. Dorland, and D. Shumaker, *Phys. Plasmas* **12**, 122305 (2005).
7. N. Joiner, D. Applegate, S. Cowley, W. Dorland, and C. Roach, *Plasma Phys. Contr. Fusion* **48**, 685 (2006).
8. M. Rosenbluth, and F. Hinton, *Phys. Rev. Lett.* **80**, 724 (1998).
9. F. Hinton, and M. Rosenbluth, *Plasma Phys. Contr. Fusion* **41**, A653 (1999).
10. H. Biglari, P. Diamond, and P. Terry, *Phys. Fluids B* **2**, 1 (1990).
11. T. Hahm, *Phys. Plasmas* **1**, 2940 (1994).
12. Y. Chen, and S. Parker, *J. Comput. Phys.* **189**, 463 (2003).
13. Y. Chen, and S. Parker, *J. Comput. Phys.* **217**, in press (2006).
14. S. Parker, C. Kim, and Y. Chen, *Phys. Plasmas* **6**, 1709 (1999).
15. A. Dimits, G. Batemen, M. Beer, B. Cohen, W. Dorland, G. Hammett, C. Kim, J. Kinsey, M. Kotschenreuther, A. Kritz, L. Lao, J. Mandrekas, W. Nevins, S. S. Parker, A. Redd, D. Shumaker, R. Sydora, and J. Weiland, *Phys. Plasmas* **7**, 969 (2000).
16. P. Diamond, M. Rosenbluth, F. Hinton, M. Malkov, J. Fleischer, and A. Smolyakov, *Plasma Physics and Controlled Nuclear Fusion Research* **IAEA-CN-69**, TH2/1 (1998).
17. W. Dorland, and G. Hammett, *Phys. Fluids B* **5**, 812 (1993).
18. L. Chen, Z. Lin, and R. White, *Phys. Plasmas* **7**, 3129 (2000).